

## Overtone atomic force microscopy studies of decagonal quasicrystal surfaces

T Drobek, R W Stark, M Gräber and W M Heckl<sup>‡</sup>

Universität München, Institut für Kristallographie, Thersienstr. 41, 80333 München, Germany

E-mail: [w.heckl@lrz.uni-muenchen.de](mailto:w.heckl@lrz.uni-muenchen.de)

*New Journal of Physics* 1 (1999) 1.1–1.11 (<http://www.njp.org/>)

Received 25 March 1999; online ?? August 1999

**Abstract.** The surface of a decagonal Al–Ni–Fe quasicrystal was investigated by overtone AFM, a special type of force modulation microscopy (FMM), where the cantilever is driven at a frequency higher than the fundamental flexural mode of the cantilever in contact with the surface. The resonance behaviour of the cantilever sample system was studied with finite element analysis (FEA). Using the excitation frequency of a torsional vibration of the cantilever, an image contrast could be obtained, which is dominated by the shear stiffness of the material. Differently orientated decagonal grains, as well as phase segregation lamellae could be resolved on the quasicrystalline specimen. It is shown that the elastic anisotropy of the material gives rise to the contrast formation in overtone microscopy.

### 1. Introduction

Since the discovery of quasicrystals in 1984 [1], their properties have been subject to a large number of studies. Although the structure of quasicrystalline materials is not yet completely understood, the knowledge of how quasiperiodic order determines the material properties has rapidly developed in recent years [2, 3]. Several experiments probing the mechanical properties of decagonal quasicrystals have been reported [4]–[6]. For all technical applications, the surface characteristics of the quasicrystals play an important role. The frictional behaviour of Al–Cu–Fe(–Cr, Si) and coatings were studied [7]. More recently, the frictional and wear behaviour of Al–Cu–Fe(–B) were investigated [8]. As a result, decagonal quasicrystals are very stiff and brittle with elastic moduli in the order of 200 GPa and show a slight elastic anisotropy of about 10%.

For atomic force microscopy (AFM) a wide variety of operational modes for measuring the different material properties of surfaces (e.g. stiffness and adhesion) has been developed. The

<sup>‡</sup> Corresponding author; Telephone/Fax: ++49-89-23944331.

elasticity of a sample can be determined directly by indentation measurements for materials which are soft in comparison with the spring constant of the cantilever [9]–[11]. Dynamic methods such as force modulation microscopy (FMM) become especially useful for the investigation of stiff materials [12]–[18]. In FMM, the cantilever vibrates while the tip is in permanent contact with the surface during scanning. Amplitude and phase of the cantilever motion are recorded and reflect mainly sample viscoelasticity. In contrast to static indentation experiments, high dynamic loads are available, while the absolute indentation amplitudes remain small. Differences in the elastic behaviour of the samples result in a shift of the resonance frequency of the surface coupled cantilever [13]. Beyond imaging of multicomponent materials there were several recent attempts to interpret the data quantitatively [14]–[16]. In the high frequency range—in this context frequencies higher than the fundamental resonance frequency—the contributions of higher flexural modes become significant [19], which leads to an evasive movement of the tip along the surface. In [17] the effect of lateral contact stiffness is discussed for conventional FMM. Recently, a careful study on the effect of springs and dashpots coupled to the end of cantilever beams with a special focus on the role of lateral forces was published [18].

In this paper, a numerical analysis of the mechanical resonance behaviour of the cantilever is presented, using finite element description of the cantilever geometry. The advantage of overtone excitation for imaging of elasticity and shear stiffness of stiff materials is discussed in particular. The method of overtone AFM is applied to Al–Ni–Fe quasicrystal surfaces in order to distinguish between different metallurgical phases and different crystallographic orientations of the quasicrystalline grains in an ingot. The difference in crystallographic orientation provides a good means of investigating the imaging process of overtone AFM because of the otherwise very similar material properties.

## 2. Materials and methods

The quasicrystal was prepared by cooling a melt of 71.5 at% Al, 23.5 at% Ni and 5 at% Fe. Then, the alloy compound was annealed for 51 hours at 900°C and quenched afterwards [20]. Several other grains of the same ingot were characterized with synchrotron x-ray diffraction analysis, revealing a decagonal structure [21]. The sample investigated by AFM was first characterized by x-ray diffraction which showed two differently orientated decagonal grains. The surface normals of these grains were tilted  $40 \pm 5^\circ$  (grain 1) and  $70 \pm 5^\circ$  (grain 2) versus the tenfold axis, respectively. Examination with electron probe microanalysis (EPMA, Cameca SX50) yielded a similar composition of 70.1 at% Al, 24.2 at% Ni and 5.7 at% Fe ( $\pm 0.4$  at% each) on both decagonal grains. The results of x-ray diffraction and EPMA prove the quasicrystalline nature of the sample. In contrast, the intermediate region between both grains contains non quasicrystalline phases with more Al but less Ni and Fe atoms. The composition, as well as the material contrast obtained by backscattering electron microscopy within this region, indicate the existence of several other phases. This area of the sample contains most probably a phase mixture of  $\text{Al}_3\text{Ni}$ ,  $\text{Al}_{13}(\text{Fe},\text{Ni})_4$  and quenched melt as concluded from the ternary phase diagrams of the Al–Ni–Fe system [22, 23]. For AFM characterization, the sample was mechanically polished to optical quality and subsequently chemically treated with a metallurgical polish (96 vol% Struers OP-S, 2 vol%  $\text{H}_2\text{O}_2$ , 2 vol% liquid ammonia).

AFM data were obtained with a modified commercial instrument as illustrated in Figure 1 (Topometrix Explorer, dry scanner, 130  $\mu\text{m}$  scan range and 10  $\mu\text{m}$   $z$ -range). All experiments were performed in ambient conditions. The cantilever was excited by direct modulation of

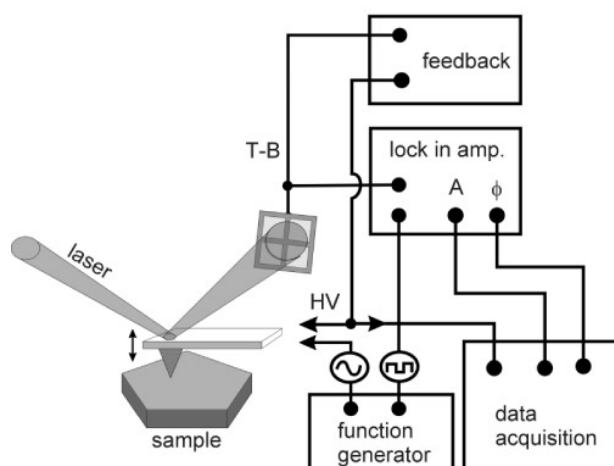


**Figure 1.** Experimental setup of the AFM. In addition to the scanning motion, the cantilever base is modulated vertically with respect to the sample by direct modulation of the  $z$ -piezo. The resulting deflection of the cantilever, detected by an optical lever system and a quadrant photo diode, is demodulated by a lock in amplifier, which passes the amplitude and phase to the data acquisition system of the AFM.

the  $z$ -scanner with a typical modulation amplitude of 0.1 Vpp (function generator: Stanford Research Systems DS 345). The deflection of the cantilever was detected by an optical lever system and a quadrant photodiode. The signals of the photodiode were demodulated by a lock-in amplifier (Stanford Research Systems SR 844). All experiments were performed with a single cantilever (Park Scientific Instruments, sharpened Microlever,  $\text{Si}_3\text{N}_4$ , v-shaped, nominal spring constant  $c = 0.1 \text{ Nm}^{-1}$ , resonant frequency nominal  $f_0 = 38 \text{ kHz}$ , measured 31.5 kHz, tip radius  $r_{\text{tip}} = 20 \text{ nm}$ ).

The finite element analysis was carried out using the static and modal analysis tools of the commercial software package Ansys 5.4 running on an IBM-SP2 workstation at the Leibnitz Rechenzentrum, München, Germany.

### 3. Theory

#### 3.1. A model for the cantilever in contact with the surface

In force modulation microscopy, the cantilever is in permanent contact with the sample surface. During scanning the cantilever base is oscillated, pressing the tip periodically into the sample. The amplitude and phase of the tip movement give information about the mechanical properties of the sample.

In order to get a realistic description of the mechanical behaviour of the system, the cantilever was modeled by finite element analysis. In figure 2(a) the true geometry of the cantilever and the mesh are shown. The elastic modulus for the gold coated cantilever was obtained by the method of effective stiffness as suggested by Hazel [24]. For the cantilever an effective Young's modulus of  $E = 150 \text{ GPa}$  was obtained for the gold coated silicon nitride. The cantilever geometry was

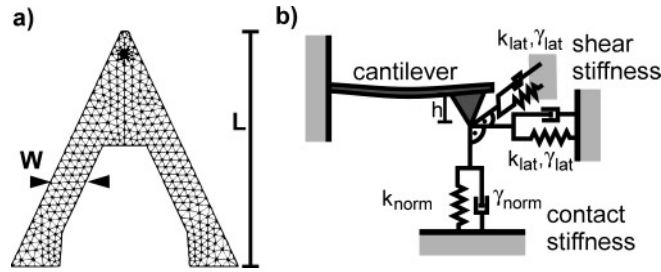


**Figure 2.** Model for a v-shaped cantilever with the tip in permanent contact with the sample. (a) The geometry used for the finite element calculations. Cantilever length  $L = 140 \mu\text{m}$ , width  $W = 18 \mu\text{m}$ , tip height  $h = 3 \mu\text{m}$ . The mesh used for the finite element analysis is also shown. (b) The sample is modelled as a tripod of spring-dashpots, which represent the contact stiffness ( $k_{\text{norm}}$ ) and the shear stiffness ( $k_{\text{lat}}$ ) and the damping of the sample. The parameters for the springs are set individually.

adjusted slightly within the limits given by the manufacturer in order to reproduce the first four measured resonant frequencies in air. Mesh refinement was performed in order to verify the mesh independence of the solutions.

The resonant spectrum of the v-shaped cantilever was calculated solving the eigenvalue problem

$$\mathbf{M} \ddot{\mathbf{q}} + \mathbf{K} \mathbf{q} = \mathbf{0}. \quad (1)$$

$\mathbf{M}$  and  $\mathbf{K}$  are the mass and the stiffness matrix; the vector  $\mathbf{q}$  denotes the nodal translation vector. The model cantilever reproduces the behaviour of the freely vibrating cantilever very well, when about 2% frequency shift is taken into account for air damping in the experiment. As a result, the spring constant of the cantilever is  $c_{\text{norm}} = 0.14 \text{ N/m}$  (nominal value:  $c_{\text{norm}} = 0.10 \text{ N/m}$ ), the lateral torsional spring constant is  $c_{\text{tor}}^{\phi} = 0.63 \text{ mNm/rad}$  (for a tip length of  $3 \mu\text{m}$  this is  $c_{\text{tor}} = 14.5 \text{ N/m}$ ), and a bending spring constant of  $c_{\text{bend}}^{\phi} = 112 \text{ mNm/rad}$  (the force acts in the axis of the cantilever onto the tip; a tip length of  $3 \mu\text{m}$  yields  $c_{\text{bend}} = 0.08 \text{ N/m}$ ).

When the cantilever is in contact with the sample, the freedom of movement of the tip is restricted by the sample stiffness. In figure 2(b) this is characterised by an effective spring constant of the tip sample contact  $k_{\text{norm}}$  in the direction normal to the sample surface, which is obtained by linear approximation of the contact stiffness from the Hertzian theory, which treats two elastic spheres in mechanical contact. Assuming a sphere with  $r_{\text{tip}} = 20 \text{ nm}$  radius and the second with an infinite radius leads to a simple model for the tip sample contact. The effective stiffness  $E_{\text{eff}}$  of the tip sample contact is given by the respective Young's moduli  $E$  and Poisson ratio  $\nu$  of tip and sample:

$$E_{\text{eff}} = \left[ \frac{(1 - \nu_{\text{tip}}^2)}{E_{\text{tip}}} + \frac{(1 - \nu_{\text{sample}}^2)}{E_{\text{sample}}} \right]^{-1}. \quad (2)$$

The static indentation  $d$  of the tip into the specimen under a certain loading force  $F$  can be derived from

$$d = \left[ \frac{9}{16} \frac{F^2}{E_{\text{eff}}^2} r_{\text{tip}} \right]^{1/3}. \quad (3)$$

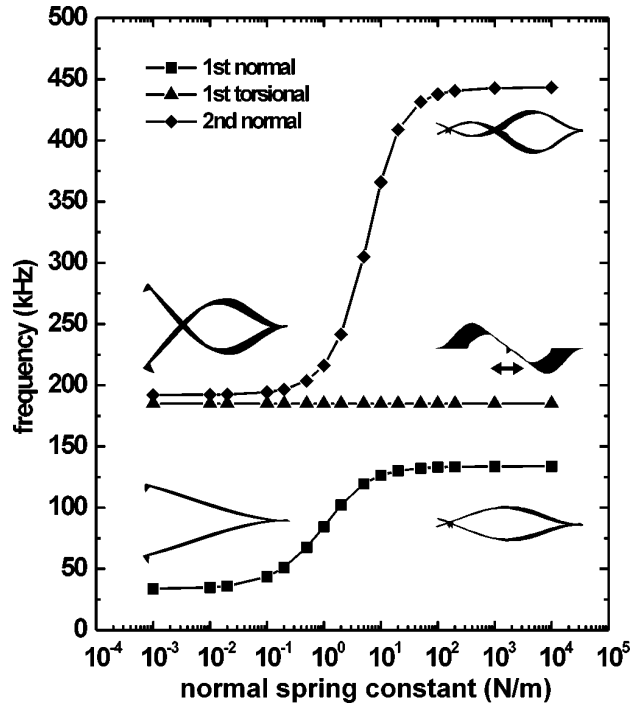


**Figure 3.** Eigenfrequencies of the first three eigenmodes in dependence of the spring constant perpendicular to the specimen. The lateral stiffness is set to zero. The modal shapes are depicted in the small inserts. The effective stiffness of the quasicrystal sample is in the order of  $k_{\text{norm}} = 350 \text{ N/m}$ . This means no image contrast based on differences in the normal stiffness can be expected.

The effective normal spring constant is the derivative of equation 3 at a certain static load  $F_0$

$$k_{\text{norm}} = \left. \frac{\partial d(F)}{\partial F} \right|_{F=F_0} = [6 E_{\text{eff}}^2 F_0 r_{\text{tip}}]^{1/3}. \quad (4)$$

For the experimental situation,  $F_0 = 30 \text{ nN}$ ,  $r_{\text{tip}} = 20 \text{ nm}$ ,  $E_{\text{eff}} \approx 100 \text{ GPa}$  an effective spring constant of roughly  $k_{\text{norm}} = 360 \text{ N/m}$  is obtained. A more elaborate model can easily be derived from the Johnson–Kendall–Roberts theory, which also includes the adhesion between tip and sample [25].

However, this one-dimensional approximation does not include lateral stiffness of the sample. In order to get a more realistic picture of the tip specimen contact, both lateral and normal sample stiffness were introduced into the model (figure 2(b)). Three different and respectively perpendicular orientated springs are fixed to the tip and allow a realistic simulation of the sample. The lateral springs introduce a torque to the end of the cantilever beam.

In the following discussion it is shown that the lateral stiffness of the specimen has serious influence on the resonant frequencies and therefore on the contrast obtained with overtone AFM on stiff materials.

First, the effect of the normal stiffness, i.e. perpendicular to the sample surface, is investigated. For the calculation, the spring constants of the lateral springs were set to zero, so that the tip can glide on the specimen surface. The eigenfrequency of the first three eigenmodes of the cantilever as a function of the contact stiffness is shown in figure 3. The small inlays illustrate

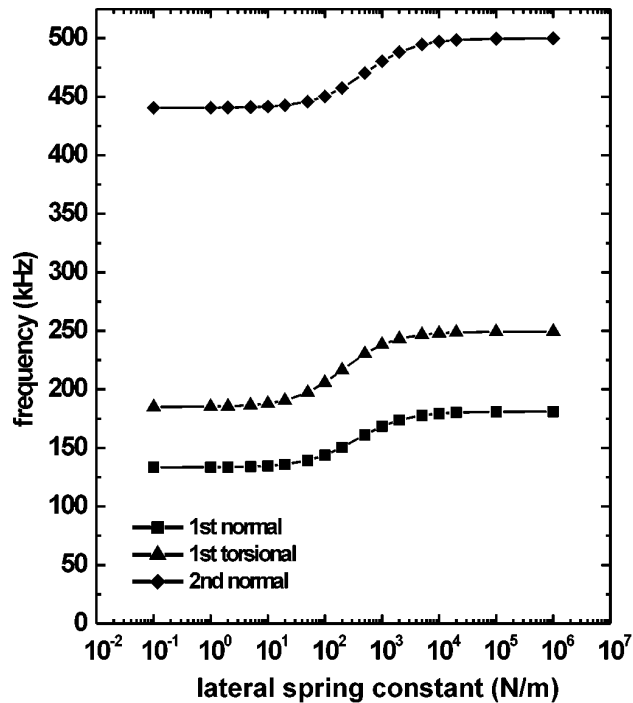


**Figure 4.** Eigenfrequencies of the first three eigenmodes in dependence of the springs parallel to the specimen. The normal stiffness is set to  $k_{\text{norm}} = 350$  N/m. The normal (symmetric) modes depend only on the spring parallel to the axis of the cantilever, the torsional (antisymmetric) modes only on the lateral stiffness.

the modal shapes. In the first eigenmode, the two cantilever arms are bent symmetrically and the tip oscillates mainly in the normal direction with respect to the sample. In contrast, the second eigenmode is an antisymmetric mode where the two arms of the cantilever vibrate oppositely. This leads to a torsion of the cantilever and a lateral movement of the tip. The third eigenmode is again a normal mode. It is worth noting that the torsional mode is independent from the stiffness in the normal direction, as could be expected from the antisymmetric bending shape.

With a very small stiffness  $k_{\text{norm}} = 10^{-3}$  N/m the cantilever vibration is similar to the vibration of a free cantilever. When the spring gets stiffer, one notes that the eigenfrequencies of the normal modes increase, whereas the eigenfrequencies of the torsional vibrations are not affected. This leads to the fact, that the eigenfrequencies of the first torsional mode and the second normal mode, which nearly coincide for a freely vibrating cantilever, are well separated for a stiff tip sample contact. In the range of  $k_{\text{norm}} = 0.1 \dots 10$  N/m the eigenfrequencies of the normal modes are very sensitive to the spring stiffness. This is the same order of magnitude as the normal force constant  $c_{\text{norm}}$  of the cantilever. Assuming a tip radius  $r = 20$  nm, a contact stiffness in this order of magnitude is obtained for biological samples or polymers. For harder samples such as metallurgical compounds, the contact stiffness is in the order of  $k_{\text{norm}} = 200$  N/m or more. In this range the modes are insensitive to differences in contact stiffness. Therefore an image contrast based on local differences in the normal stiffness cannot be expected for stiff materials. However, in the normal modes a bending appears and the tip performs an evasive movement along the surface which is influenced by the lateral stiffness of the sample.

Assuming a laterally confined tip, the eigenfrequencies as functions of the lateral (x and y)

stiffness is plotted in figure 4. The normal spring constant is set to  $k_{\text{norm}} = 350$  N/m, which reflects the experimental situation. For small lateral spring constants and for very stiff ones, the eigenfrequencies are nearly constant, whereas in the range of  $k_{\text{lat}} = 100 \dots 1000$  N/m, both the eigenfrequencies of the normal as well as the torsional modes are increasing with the stiffness. The eigenfrequencies of the normal modes are dependent on the spring in direction parallel to the cantilever axis ( $y$ ) and independent on the lateral spring ( $x$ ). In contrast, the torsional modes only depend on the numerical value of the spring perpendicular to the cantilever axis ( $x$ ).

Several conclusions can be drawn from this result:

- The normal flexural modes strongly depend on the sample shear stiffness in the direction of the cantilever, not only on the Young's modulus. If the modulation amplitude is kept very small, the tip does not overcome static friction and is restricted laterally. As a consequence, the image contrast is based on both Young's modulus and shear stiffness. For larger amplitudes the situation becomes more complicated because a stick slip process has to be investigated. Then, frictional properties of the sample also play an important role.
- The eigenfrequency of the torsional mode only depends on the lateral stiffness of the sample and is therefore predestinated as a sensing mode for shear stiffness.
- The eigenfrequencies of the torsional modes are highly sensitive to the lateral sample stiffness in a range which is typical for metallurgical compounds.

### 3.2. Image contrast

For the interpretation of the amplitude and phase signal, the torsionally vibrating cantilever can be described as an harmonic oscillator, which is driven externally at a fixed frequency  $\omega$  with an excitation amplitude  $a_0$ . Now, the image contrast can be understood by investigation of amplitude  $A$  and phase  $\varphi$ :

$$A = \frac{a_0}{k} \left[ \left( 1 - \left[ \frac{\omega}{\omega_0} \right]^2 \right)^2 + \left( 2\gamma \frac{\omega}{\omega_0} \right)^2 \right]^{-1/2} \quad (5)$$

$$\varphi = \arctan \left[ \frac{2\gamma \omega / \omega_0}{1 - (\omega / \omega_0)^2} \right] \quad (6)$$

In a first order approximation, the sample is characterized by its local lateral (shear) stiffness and damping. The parameters are the resonant frequency  $\omega_0$ , the effective spring constant  $k$  for the cantilever torsion, and the damping coefficient  $\gamma$ . An increasing shear stiffness increases the lateral spring constant and consequently the resonant frequency of the system. For a v-shaped cantilever this can be calculated by finite element analysis, as discussed in section 3.1.

Therefore, the local values of the amplitude and the phase are used as image information in the scanning process. Damping is introduced by tip slip friction and intrinsic damping in the tip-sample contact. As can be seen in equations 5 and 6, both factors, intrinsic damping which determines  $\gamma$  and sample stiffness determining  $k$  and  $\omega_0$ , contribute to the image contrast. In experiment,  $\omega_0$  and  $\gamma$  can be measured directly by performing a frequency sweep on a definite position in order to obtain information about the sample characteristics  $k_{\text{lat}}$  and  $\gamma$ . The image obtained at a constant driving frequency  $\omega$  near the resonant frequency  $\omega_0$  of the surface coupled cantilever provides information about the material distribution on the sample surface. Damping is caused by friction processes on the surface, as well as other effects of energy dissipation, for

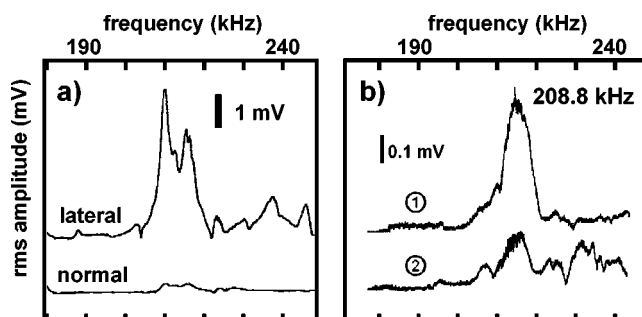


**Figure 5.** Cantilever overtone frequency spectra taken with the tip in contact with the specimen. In (a) the amplitude of the first torsional resonance is shown, measured with (1) the lateral bending and (2) the normal bending signal of the cantilever. In (b) the amplitude of the normal bending signal is compared at two different locations (indicated in figure 6(a)). The amplitude of the torsional resonance at 208.8 kHz exhibits different heights depending on the location of contact, as well as a small frequency shift of about 1 kHz. This material dependent resonance behaviour is used for imaging.

example phonon excitations in the sample material, which can be strongly dependent on the crystallographic orientation of the material. In order to minimize the influence of friction, only very small amplitudes should be employed for shear stiffness measurements.

#### 4. Experimental results and discussion

The experiment was carried out on a polycrystalline Al–Ni–Fe specimen described in section 2. The area examined in this experiment consists of two differently orientated decagonal grains and an intermediate region containing a mixture of more aluminium rich phases. The resonant frequency of the first torsional eigenmode was used in order to get high signal amplitudes in combination with small tip movements.

As a first step, frequency spectra of the tip in contact with the specimen were taken. In figure 5(a) the amplitude of the first torsional resonance is shown, measured with the lateral and the normal bending signal of the cantilever at a fixed position on grain 2. In figure 5(b) the amplitude of the lateral bending signal in the frequency region of the first torsional resonance is compared at two different locations on the two decagonal grains (indicated in figure 6(a)). Here a small frequency shift of about 1 kHz for the resonant frequency between the two grains appears, as well as a significant difference of the resonance amplitude.

In the next step, the cantilever response at 208.8 kHz, which is the peak frequency on the first grain, was used for image formation. Figure 6(a) shows the amplitude image, figure 6(b) the corresponding phase. In both pictures, there is a significant contrast between both grains (numbers 1 and 2 as indicated in figure 6(a)), the boundaries between the decagonal grains and the aluminium rich intermediate region are sharp edges.

The topographic AFM image is shown in figure 6(c). An almost invisible step of 5 nm height (arrows) is the only topographic sign of the grain boundary. The topographic contrast between the decagonal grain and the intermediate material is smaller than the average surface roughness ( $R_{\text{rms}} = 33$  nm) induced by the preparation process.

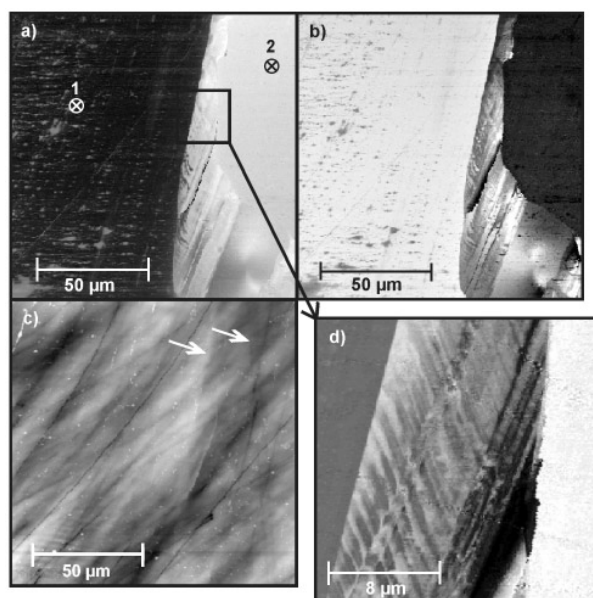


**Figure 6.** Simultaneously obtained AFM data of the Al–Ni–Fe sample. (a) Overtone amplitude, (b) phase of the cantilever deflection at 208.8 kHz and (c) topography. In the topographic image, the grain boundaries which are clearly visible in (a) and (b) appear as tiny steps of about 5 nm height (arrows). The numbers in a) indicate the locations where the frequency response spectra (figure 5(b)) were measured. Part (d) shows an overtone amplitude image (208.8 kHz) of the aluminium rich region between both grains. Greyscales black to white: a) amplitude 30 % to 100 %, (b) phase angle 0 to 80°, (c) topography 0 to 230 nm, (d) amplitude 30 % to 100 %.

Figure 6(d) shows a zoom into the intermediate region (amplitude of the torsional resonance). The material exhibits striped inhomogeneities on the scale of several tens of microns, which are not detectable in the topography. The lamellae structure of the phase mixture found in this area is a common phenomenon in metallic phase mixtures. For the Al–Ni–Fe system, similar exsolution lamellae are described in [23].

In order to verify the origin of the image contrast in overtone AFM, friction force measurements were performed. In the aluminium rich intermediate region between the two grains, the friction is slightly (3%) increased as compared to the decagonal grains. The difference in the frictional forces occurring on the two decagonal grains is below 0.1% (data not shown). Therefore, a contrast mechanism in force modulation based on the frictional behaviour like a tip slip effect [13, 26] can be excluded here. Force spectroscopy measurements (force versus distance recording) showed a similar adhesion behaviour on the two decagonal grains, so that an adhesion mechanism cannot be excluded either (IS THIS OK?).

From the measured resonant frequencies on the two Al–Ni–Fe grains the shear stiffness values of 180 N/m and 200 N/m can be obtained. The only difference between these two grains is the crystallographic orientation of the surface. A detailed analysis of the elastic behaviour of decagonal Al–Ni–Co quasicrystals was performed by Chernikov *et al* [6]. Assuming similar elastic properties for decagonal Al–Ni–Fe quasicrystals, the material shows a difference of the

Young's moduli for the two orientations of about 7%, whereas the difference of the shear moduli is of the order of 10%. As discussed in section 3.1, for stiff materials the frequencies of the torsional as well as the normal resonances are not sensitive to the contact stiffness i.e. the Young's modulus. This means that the difference of the shear modulus and the damping behaviour in the lateral direction is responsible for the image contrast in overtone AFM image formation. For anisotropic materials this fact can be used to distinguish between differently orientated grains in a simple way.

## 5. Conclusions

In this paper overtone AFM, a new force modulation mode employing frequencies well above the fundamental eigenfrequency of the clamped, pinned cantilever system is introduced. The mechanical resonances of the cantilever sample system were analysed and found to be characteristic for the shear stiffness of the sample. The first torsional resonance of the cantilever was employed for imaging. Here the lateral stiffness is well separated from the normal contact stiffness i.e. Young's modulus, which is important for the investigation of stiff materials. On a polycrystalline Al–Ni–Fe quasicrystal sample, an interphase consisting of a phase mixture of non quasicrystalline  $\text{Al}_3\text{Ni}$  and  $\text{Al}_{13}(\text{Fe}, \text{Ni})_4$  exhibiting a characteristic lamellae structure between two decagonal grains could clearly be identified by overtone AFM. The image contrast between both differently oriented decagonal grains is based on the anisotropy of the shear modulus and the damping behaviour

The overtone microscopy has the potential to become a powerful member of the family of scanning probe techniques, especially suitable for investigation of metallurgical multicomponent systems with high spatial resolution.

## Acknowledgments

We thank Scientific Instruments GmbH Germany for supplying the lock-in amplifier for test purposes, Dr B Grushko (Forschungszentrum Jülich, Germany) for providing the quasicrystalline specimen, G Schrag and P Scheubert (Technische Universität München, Germany) for the introduction to the Ansys program. This work was supported by DFG Grant He-1617/7-1 (TD) and Bayerische Forschungsförderung (RWS).

## References

- [1] Shechtman D, Blech I, Gratias D and Cahn J W 1984 *Phys. Rev. Lett.* **53** 1951
- [2] Quilichini M and Janssen T 1997 *Rev. Mod. Phys.* **69** 277
- [3] Ebinger W, Roth J and Trebin H-R 1998 *Phys. Rev. B* **58** 8338
- [4] Wittmann R, Urban K, Schandl M and Hornbogen E 1991 *J. Mater. Res.* **6** 1165
- [5] Feuerbacher M, Bartsch M, Grushko B, Messerschmidt U and Urban K 1997 *Philos. Mag. Lett.* **76** 369
- [6] Chernikov M A, Ott H R, Bianchi A, Milgiori A and Darling T W 1998 *Phys. Rev. Lett.* **80** 321 (1998)
- [7] Kang S S, Dubois J M and von Stebut J 1993 *J. Mater. Res.* **8** 2471 (1993)
- [8] Singer I L, Dubois J M, Soro J M, Rouxel D and von Stebut J 1997 *Proc. 6th Int. Conf. on Quasicryst.* 769
- [9] Radmacher M, Fritz M and Hansma P K 1995 *Int. Biophys. J.* **69** 264
- [10] Stark R W, Thalhammer S, Wienberg J and Heckl W M 1998 *Appl. Phys. A* **66** S579
- [11] Stark R W, Drobek T, Weth M, Fricke J and Heckl W M 1998 *Ultramicroscopy* **75** 161

- [12] Radmacher M, Tilmann R W and Gaub H E 1993 *Biophys. J.* **64** 735
- [13] Troyon M, Wang Z, Pastre D, Lei H N and Hazotte A 1997 *Nanotechnology* **8** 163
- [14] Burnham N A, Gremaud G, Kulik A J, Gallo P J and Oulevey F 1996 *J. Vac. Sci. Technol. B* **14** 1308
- [15] DeVechio D and Bushan B 1997 *Rev. Sci. Instrum.* **68** 4498
- [16] Yamanaka K and Nakano S 1998 *Appl. Phys. A* **66** S313
- [17] Mazeran P-E and Loubet J-L 1997 *Tribology Lett.* **3** 125
- [18] Rabe U, Turner J and Arnold W 1998 *Appl. Phys. A* **66** S277
- [19] Stark R W, Drobek T and Heckl W M 1999 *Appl. Phys. Lett.* **74** 3296
- [20] Sample id NF10, Grushko B, Forschungszentrum Jülich, Germany
- [21] Weidner E and Frey F *unpublished data*
- [22] Lemmerz U, Grushko B, Freiburg C and Jansen M 1994 *Phil. Mag. Lett.* **69** 141
- [23] Grushko B, Lemmerz U, Fischer K and Freiburg C 1996 *Phys. Stat. Solidi* **155** 17
- [24] Hazel J L and Tsukruk V V 1999 *Thin Solid Films* **339** 249
- [25] Johnson K L 1994 *Contact Mechanics* (Cambridge: Cambridge University Press)
- [26] Li F-B, Thompson G E and Newman RC 1998 *Appl. Surf. Sci.* **126** 21